**Electronic Supplementary Information
for**

Late first-row transition metal complexes of 17-membered piperazine-based macrocyclic ligand: structures and magnetism

Eva Zahradníková,[a] Radovan Herchel,[a] Ivan Šalitroš,[a,b] Ivana Císařová[c] and Bohuslav Drahoš[a]*

[a] Department of Inorganic Chemistry, Faculty of Science, Palacký University, 17. listopadu 12, CZ-771 46 Olomouc, Czech Republic, Fax: +420 585 634 954. Tel: +420 585 634 429. E-mail: bohuslav.drahos@upol.cz
[b] Department of Inorganic Chemistry, Faculty of Chemical and Food Technology, Slovak University of Technology in Bratislava, Bratislava SK-81237, Slovakia.
[c] Department of Inorganic Chemistry, Faculty of Science, Charles University, Hlavova 2030, 128 00 Prague, Czech Republic

Table of content:

Details of DC/AC Susceptibility Measurements

Figure S1 ^{1}H–^{13}C *gs*-HMQC NMR spectrum (400 MHz, CDCl$_3$) of **L$_{diProp}$** (1,5,13,17,22-pentaazatricyclo[15.2.2.1^{7,11}]docosa-7,9,11(22)-triene) with a residual peak of CHCl$_3$ at 7.27 ppm (^{1}H) and CDCl$_3$ at 77.0 ppm (^{13}C).
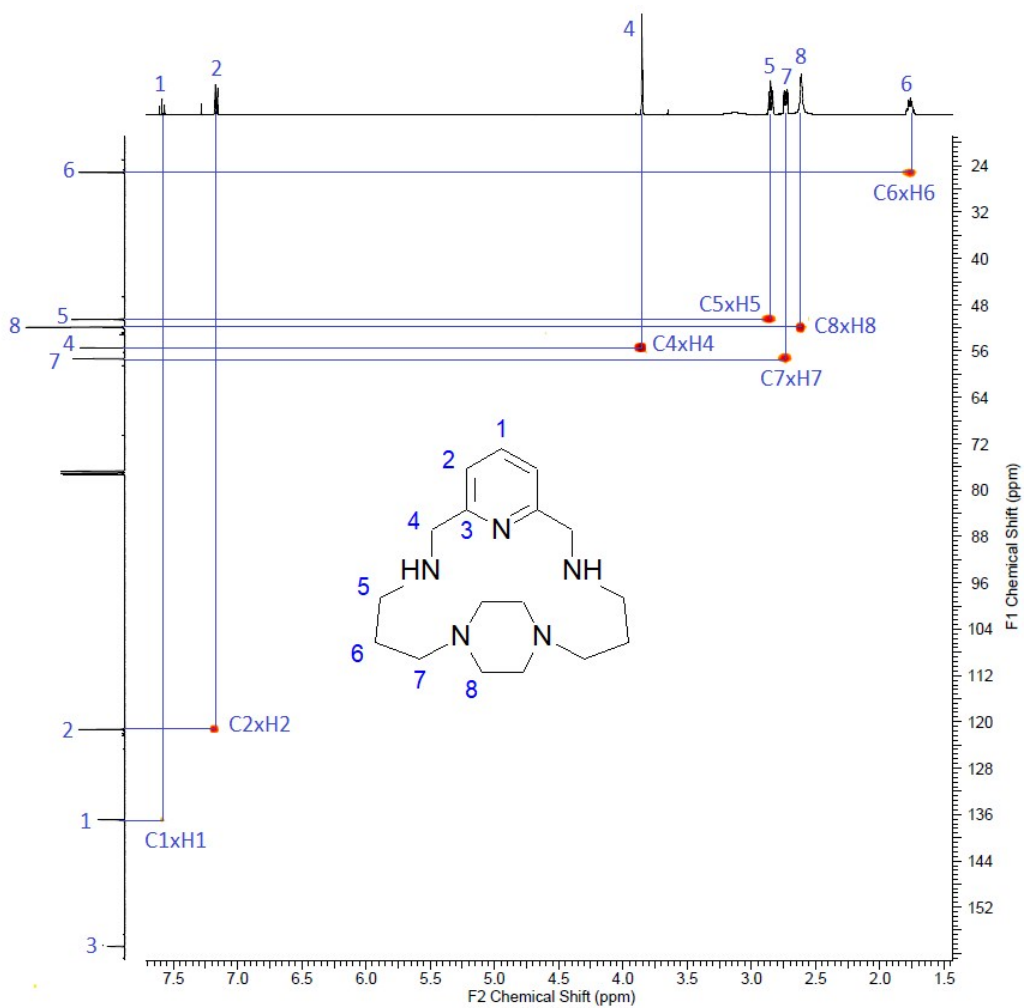
Figure S2 ^1H–^{13}C *gs*-HMBC NMR spectrum (400 MHz, CDCl$_3$) of **L$_{diProp}$** (1,5,13,17,22-pentaazatricyclo[15.2.2.1^{7,11}]docosa-7,9,11(22)-triene) with a residual peak of CHCl$_3$ at 7.27 ppm (^1H) and CDCl$_3$ at 77.0 ppm (^{13}C).
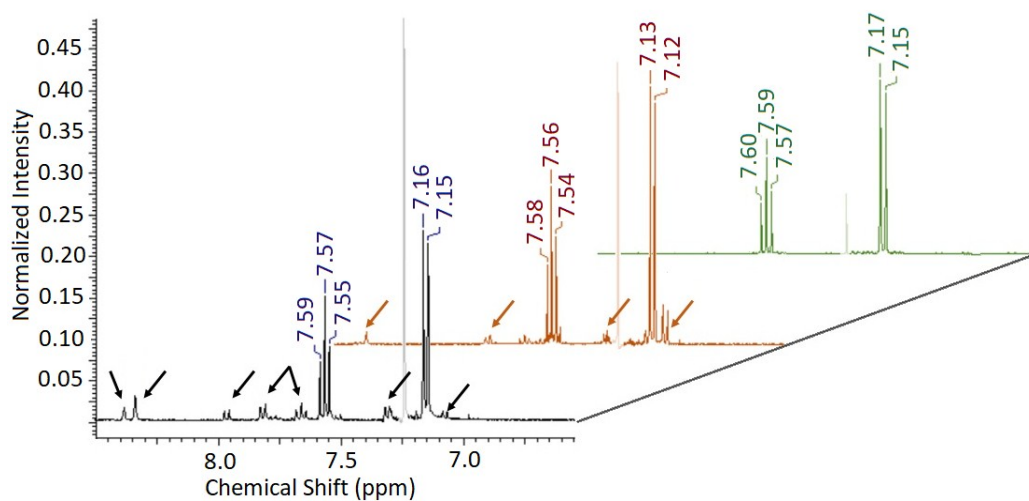
Figure S3 Selected parts of ^{1}H NMR spectra (6.5–8.4 ppm) showing signals of the aromatic pyridine ring of the ligand **L$_{diProp}$**. Black curve – obtained product when amine was added manually without linear pump. Orange curve – obtained product when amine was added by linear pump. Green curve – purified product obtained after column chromatography. Arrows indicate the impurities/side-products (according to mass spectra, a twice as large cycle and also an uncycled side products were detected).
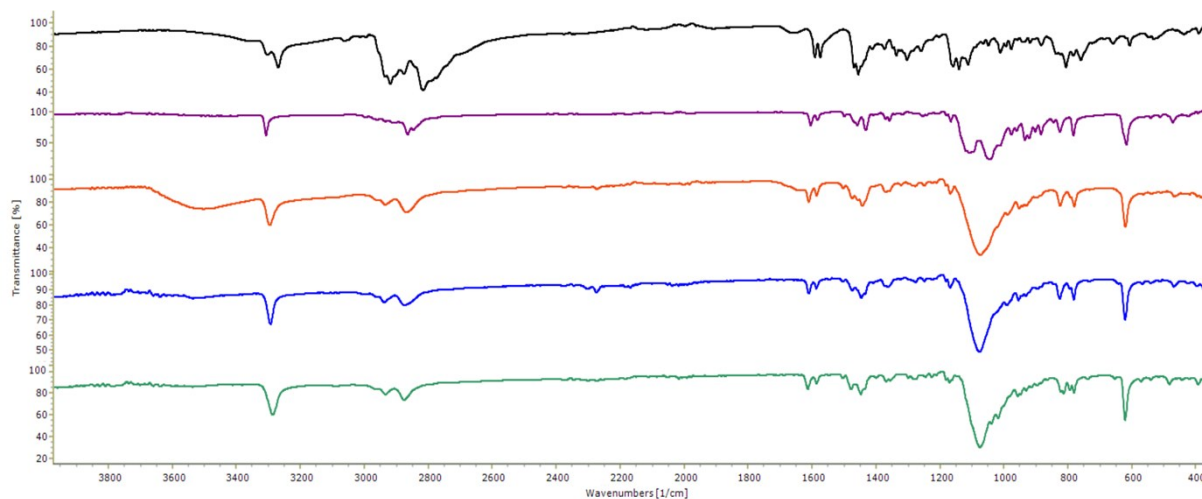
Figure S4 Comparison of IR spectra of pure ligand **L**$_{\textbf{diProp}}$ (*black*) together with spectra of its studied complexes **1** (*purple*), **2** (*orange*), **3** (*blue*) and **4** (*green*).
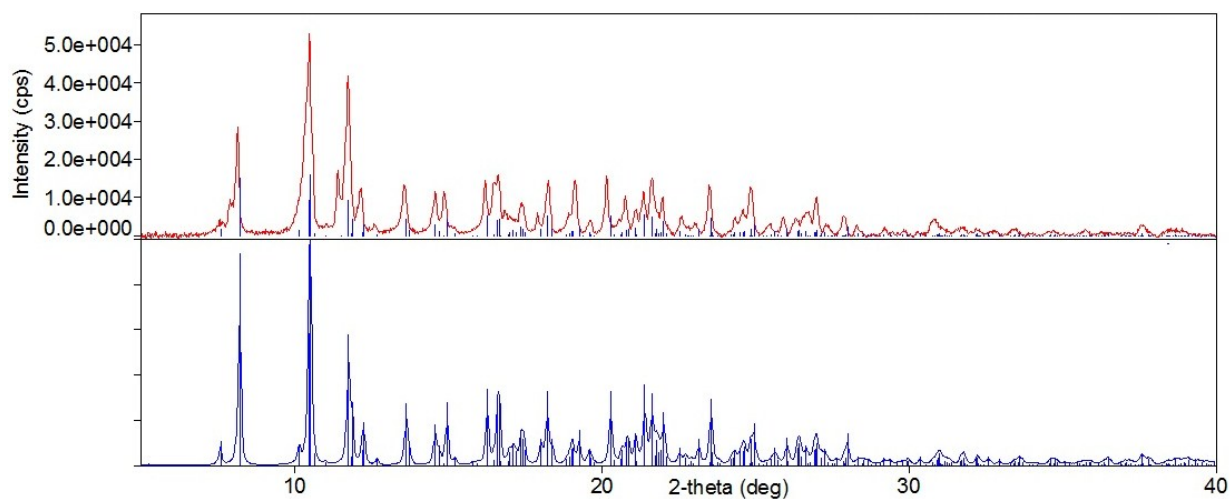
Figure S5 X-ray powder diffraction pattern of **4** (red curve – measured, blue curve – theoretically calculated patter from single-crystal X-ray data).
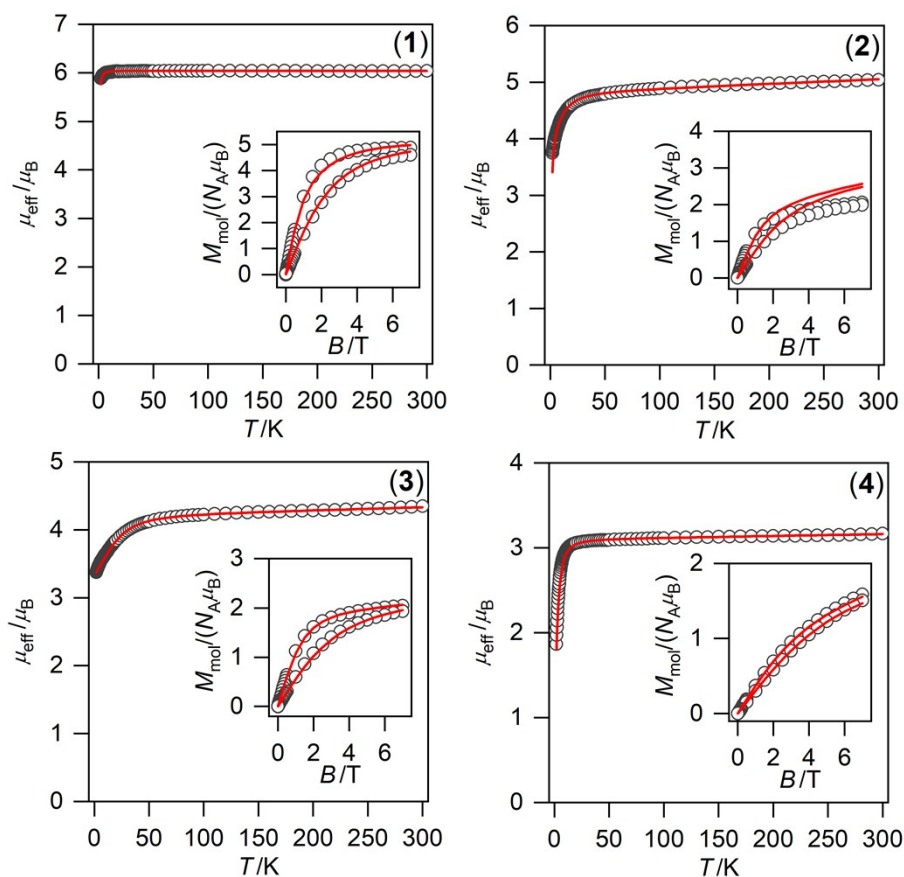
Figure S6 Magnetic data for compounds **1**–**4**. Temperature dependence of the effective magnetic moment μ_{eff} and the isothermal magnetizations M_{mol} measured at $T = 2$ and 4.6 K. The empty circles represent the experimental data points, and the full lines represent the best fits calculated by using eq. 1 with parameter sets listed in Table 3 ($D < 0$ for **1** and **4**, $D > 0$ for **2** and **3**).
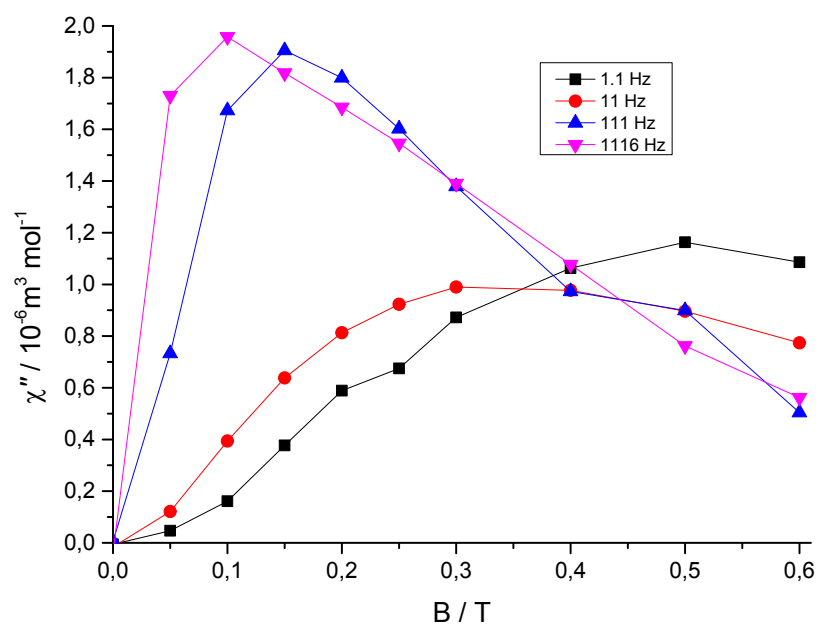
Figure S7 Mapping of the out-of-phase component (χ'') of AC susceptibility as a function of the applied external B_{DC} field for a set of four frequencies of the AC field at $T = 2.0$ K.
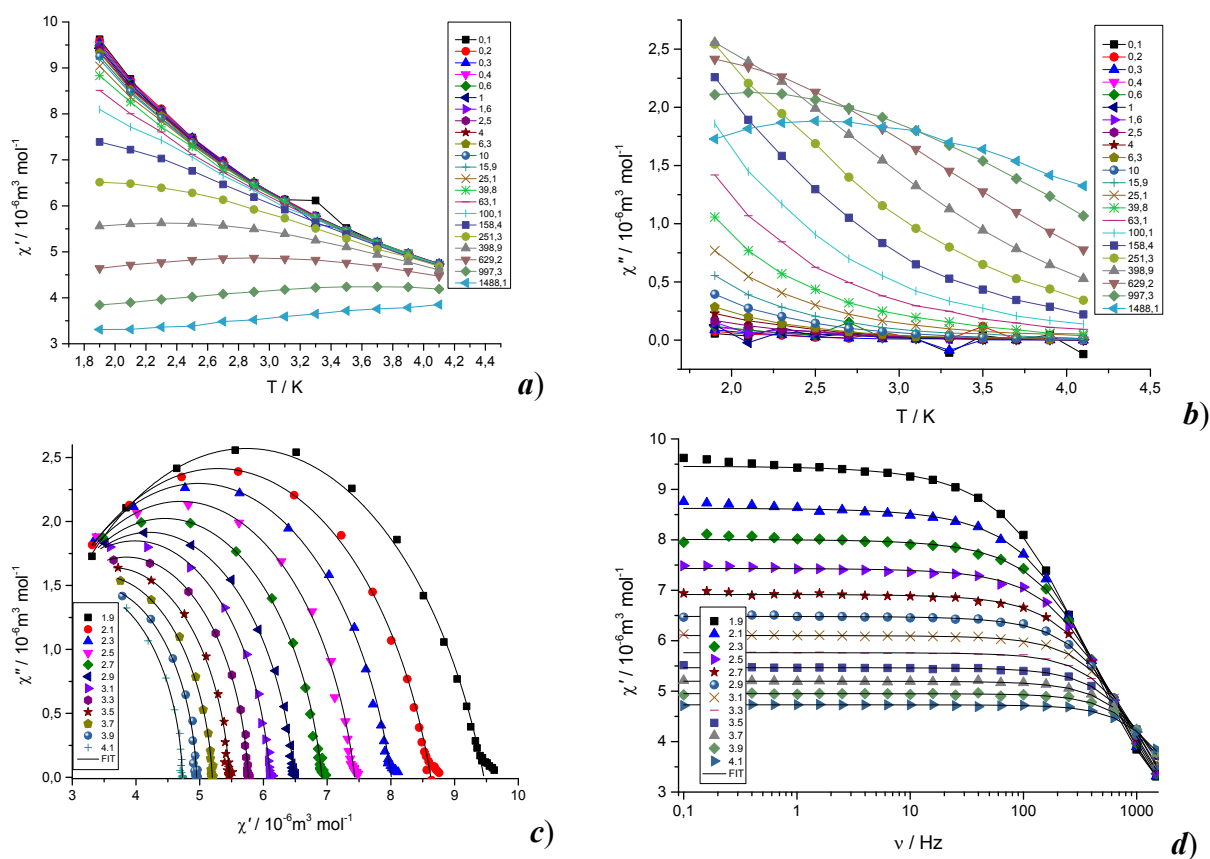
Figure S8 AC susceptibility data for **3** recorded at B_{DC} = 0.1 T: Temperature dependence of in-phase χ' (**a**) and out-of-phase χ'' (**b**) components of AC susceptibility (solid lines are only guiding for the eyes). Cole-cole diagram (**c**) and frequency dependent in-phase χ' (**d**) component of AC susceptibility (solid lines are fits).

7

Table S1 Results of continuous shape measures calculations using program Shape 2.1 for compounds **1–4**.[a]

|	Mn(II)	Fe(II)		Co(II)		Ni(II)	
CN=5[b]	Mn	Fe1	Fe2	Co1	Co1A	Ni1	Ni2
PP-5	–	–	–	–	–	10.754	10.967
vOC-5	–	–	–	–	–	10.870	10.557
TBPY-5	–	–	–	–	–	12.256	12.032
SPY-5	–	–	–	–	–	10.522	10.187
JTBPY-5	–	–	–	–	–	13.363	13.120
CN=6[c]							
HP-6	–	28.028	27.815	28.463	28.266	–	–
PPY-6	–	7.066	6.668	7.189	6.954	–	–
OC-6	–	12.576	13.111	12.547	12.849	–	–
TPR-6	–	5.471	5.410	5.257	5.140	–	–
JPPY-6	–	9.950	9.608	9.930	9.798	–	–
CN=7[d]							
HP-7	34.872	–	–	–	–	–	–
HPY-7	21.518	–	–	–	–	–	–
PBPY-7	4.643	–	–	–	–	–	–
COC-7	2.095	–	–	–	–	–	–
CTPR-7	0.971	–	–	–	–	–	–
JPBPY-7	9.320	–	–	–	–	–	–
JETPY-7	20.625	–	–	–	–	–	–

[a] The listed valued correspond to the deviation between the ideal and real coordination polyhedral, the lowest values are in red color.
[b] PP-5 = pentagon, vOC-5 = vacant octahedron, TBPY-5 = trigonal bipyramid, SPY-5 = spherical square pyramid, JTBPY-5 = Johnson trigonal bipyramid J12.
[c] HP-6 = hexagon, PPY-6 pentagonal pyramid, OC-6 = octahedron, TPR-6 = trigonal prism, JPPY-6 = Johnson pentagonal pyramid J2.
[d] HP-7 = heptagon, HPY-7 = hexagonal pyramid, PBPY-7= pentagonal bipyramid, COC-7 = capped octahedron, CTPR-7 = capped trigonal prism, JPBPY-7 = Johnson pentagonal bipyramid J13, JETPY-7 = Johnson elongated triangular pyramid J7.

Table S2 Selected bond angles (°) for the studied complexes **1–3**. Two values in case of complexes **2** and **3** are given for two crystallographically independent molecules found in the asymmetric unit.

Complex **1** Angles (°)		Complex **2** Angles (°)		Complex **3** Angles (°)	
N1–Mn–N2	73.73(6)	N1–Fe1–N2	75.3(1)	N1–Co1–N2	76.7(1)
N1–Mn–N3	145.76(7)	N1A–Fe2–N2A	75.5(1)	N1A–Co1A–N2A	77.0(1)
N1–Mn–N4	148.43(7)	N1–Fe1–N3	153.0(1)	N1–Co1–N3	152.6(1)
N1–Mn–N5	73.23(6)	N1A–Fe2–N3A	152.4(1)	N1A–Co1A–N3A	152.3(1)
N1–Mn–O1	80.88(6)	N1–Fe1–N4	135.2(1)	N1–Co1–N4	136.7(1)
N1–Mn–O5	82.41(6)	N1A–Fe2–N4A	136.7(1)	N1A–Co1A–N4A	137.55(9)
N2–Mn–N3	82.07(6)	N1–Fe1–N5	74.0(1)	N1–Co1–N5	74.44(9)
N2–Mn–N4	128.10(6)	N1A–Fe2–N5A	74.3(1)	N1A–Co1A–N5A	74.64(9)
N2–Mn–N5	146.96(6)	N1–Fe1–N6	86.7(1)	N1–Co1–N6	86.53(9)
N2–Mn–O1	96.69(6)	N1A–Fe2–N6A	86.3(1)	N1A–Co1A–N6A	86.24(9)
N2–Mn–O5	80.89(6)	N2–Fe1–N3	80.7(1)	N2–Co1–N3	80.4(1)
N3–Mn–N4	65.72(6)	N2A–Fe2–N3A	80.1(1)	N2A–Co1A–N3A	79.8(1)
N3–Mn–N5	127.49(6)	N2–Fe1–N4	115.7(1)	N2–Co1–N4	115.9(1)
N3–Mn–O1	78.25(6)	N2A–Fe2–N4A	116.1(1)	N2A–Co1A–N4A	115.7(1)
N3–Mn–O5	117.63(6)	N2–Fe1–N5	148.9(1)	N2–Co1–N5	150.8(1)
N4–Mn–N5	82.37(6)	N2A–Fe2–N5A	149.1(1)	N2A–Co1A–N5A	151.1(1)
N4–Mn–O1	113.85(6)	N2–Fe1–N6	99.9(1)	N2–Co1–N6	100.8(1)
N4–Mn–O5	79.83(6)	N2A–Fe2–N6A	100.1(1)	N2A–Co1A–N6A	101.1(1)
N5–Mn–O1	78.29(6)	N3–Fe1–N4	67.1(1)	N3–Co1–N4	67.8(1)
N5–Mn–O5	94.56(6)	N3A–Fe2–N4A	66.66(9)	N3A–Co1A–N4A	67.25(9)
O1–Mn–O5	163.11(6)	N3–Fe1–N5	130.4(1)	N3–Co1–N5	128.62(9)
		N3A–Fe2–N5A	130.78(9)	N3A–Co1A–N5A	129.04(9)
		N3–Fe1–N6	85.4(1)	N3–Co1–N6	83.2(1)
		N3A–Fe2–N6A	85.4(1)	N3A–Co1A–N6A	83.50(9)
		N4–Fe1–N5	83.36(9)	N4–Co1–N5	83.22(9)
		N4A–Fe2–N5A	82.55(9)	N4A–Co1A–N5A	82.67(9)
		N4–Fe1–N6	129.1(1)	N4–Co1–N6	126.8(1)
		N4A–Fe2–N6A	127.74(9)	N4A–Co1A–N6A	126.23(9)
		N5–Fe1–N6	83.69(9)	N5–Co1–N6	81.82(9)
		N5A–Fe2–N6A	84.46(9)	N5A–Co1A–N6A	82.67(9)

Table S3 Parameters of one-component Debye model for **3** at $B_{DC} = 0.1$ T.

T / K	χ_S / 10^{-6} m^3 mol^{-1}	χ_T / 10^{-6} m^3 mol^{-1}	α / 10^{-2}	τ / 10^{-4} s
1.9	2.00	9.46	23.10	4.34
2.1	1.94	8.62	20.36	3.33
2.3	1.95	8.01	17.39	2.80
2.5	1.97	7.43	14.89	2.35
2.7	1.99	6.91	12.45	1.99
2.9	1.93	6.48	10.94	1.69
3.1	1.86	6.10	8.71	1.41
3.3	1.95	5.76	6.51	1.29
3.5	1.82	5.47	6.78	1.07
3.7	1.70	5.20	6.66	0.90
3.9	1.75	4.95	4.41	0.80
4.1	1.61	4.72	3.84	0.66

Table S4 Relaxation parameters for compound **3** using the single Orbach, single Raman model and their combinations (using eqv. 3).

Model	B_{DC} / T	U/k_B / K	τ_0/s	C / K^{-n} s^{-1}; n	AB^m / T^{-m} K^{-1} s^{-1}	R^2
Orbach[a]	0.1	8.55±0.48	(8.89±1.31)10^{-6}	-	-	0.9780
Raman	0.1	-	-	10.67±0.56; 6.20±0.06	-	0.9945
Orbach+Direct	0.1	13.02±1.03	(4.35±1.11)10^{-6}	-	1157.33±70.87	0.9954
Raman+Direct	0.1	-	-	109.10±44.42; 3.29±0.27	786.71±135.29	0.9973

[a] for the temperature range 2.7–4.1 K.

Details of DC/AC Susceptibility Measurements

In order to prevent the random orientation of crystallites in the magnetic field, the precisely weighted complex **1–4** was introduced into the gelatin capsule, mixed with melted eicosane, homogenized and congealed. This procedure was employed for direct-current (DC) as well as for alternating-current (AC) susceptibility measurements. Obtained data were corrected for the diamagnetic contribution of the eicosane and the capsule.

All herein reported magnetic data induced by the oscillating, alternating-current (AC) magnetic field B_{AC} were taken at an amplitude of $B_{AC} = 0.38$ mT. At first, the static field (B_{DC}) scan for a limited number of frequencies over four order of magnitudes (1.1 Hz, 11 Hz, 111 Hz and 1116 Hz) was measured in order to determine the optimum B_{DC} field at which all further AC susceptibility investigations were carried out (Fig. S6).

Collected sets of χ' and χ'' susceptibilities measured in the frequency range 0.1 Hz − 1488.1 Hz (20 steps) upon the heating from 1.9 K up to 4.1 K in 0.2 K step (12 isotherms) taken at $B_{DC} = 0.1$ T were fitted using the formulas for single-channel Debye model.

$$\chi'(\omega) = \chi_S + \left(\chi_T - \chi_S\right)\frac{1+(\omega\tau)^{(1-\alpha)}\sin(\pi\alpha/2)}{1+2(\omega\tau)^{(1-\alpha)}\sin(\pi\alpha/2)+(\omega\tau)^{(2-2\alpha)}} \tag{S1}$$

$$\chi''(\omega) = \left(\chi_T - \chi_S\right)\frac{(\omega\tau)^{(1-\alpha)}\cos(\pi\alpha/2)}{1+2(\omega\tau)^{(1-\alpha)}\sin(\pi\alpha/2)+(\omega\tau)^{(2-2\alpha)}} \tag{S2}$$

Four free parameters can be retrieved reliably by using 40 experimental data points for each temperature: ω - angular frequency, τ - relaxation time, α-distribution parameter, χ_S and χ_T are adiabatic and thermodynamic susceptibilities, respectively.